Supporting information

Electrodeposition of nickel cobalt alloys from metal chloride-L-serine deep eutectic solvent for hydrogen evolution reaction

Yanling Hu, Chao Wang*

Department of Chemistry and Chemical Engineering, The Youth Innovation Team of Shaanxi Universities, Shaanxi University of Science and Technology, Xi'an, Shaanxi 710021, China

* Corresponding author:

cwang@sust.edu.cn

Content

1. Chemicals

Nickel chloride hexahydrate ($NiCl_2 \cdot 6H_2O$; Sinopharm; 98%), cobalt chloride hexahydrate ($CoCl_2 \cdot 6H_2O$; Damao; 99%), L-serine (99%, AR grade), potassium hydroxide (KOH; Guanghua; 85%), ethanol (C_2H_5OH; Guanghua; 99.7%), carbon cloth (1 × 2 cm^2), foam nickel (1 × 2cm^2), silver wire (diameter 0.5 mm), graphite rod (diameter 6mm), saturated calomel electrode (Shanghai Insea), and glassy carbon electrode (diameter 2 mm).

2. Electrochemistry

The potential reported is relative to the reversible hydrogen electrode (RHE), and the conversion equations for potential are shown in the following Eqns. (S1) - (S2)

$$E_{RHE} = E_{SCE} + 0.059*pH + 0.241 \quad \text{(S1)}$$

$$\eta_{RHE} = E_{RHE} \quad \text{(S2)}$$

E_{RHE} represents the potential relative to the reversible hydrogen electrode (RHE), E_{SCE} represents the potential relative to the saturated calomel electrode (SCE), and η represents the overpotential. with the formula shown in Eqn (S3).

$$E_{iR\text{-}corrected} = E_{RHE} - iR \quad \text{(S3)}$$

Tafel slope (b) is shown in Eqn (S4)

$$\eta = b \log j \quad \text{(S4)}$$

The double-layer capacitance (C_{dl}) was measured using cyclic voltammetry (CV) at a scan rate of 20 - 100 mV s^{-1}. All electrochemical experiments are repeated at least three times.

2. Characterization

The phase characterization studied using X-ray powder diffraction (XRD, Rigaku D/Max-3c, Japan). The microstructure of the catalyst and the elemental distribution of the samples were observed using a field emission scanning electron microscope (ZEISS Sigma 300, Germany) and an energy-dispersive X-ray spectrometer (EDX). Transmission electron microscopy (TEM) and high-resolution TEM (HRTEM) measurements were conducted using a field emission electron microscope (JEOL JEM F200, Japan). The elemental composition and valence state of the samples were determined using X-ray photoelectron spectroscopy (XPS, Shimadzu/Kratos, Japan).

3. Electrochemical deposition

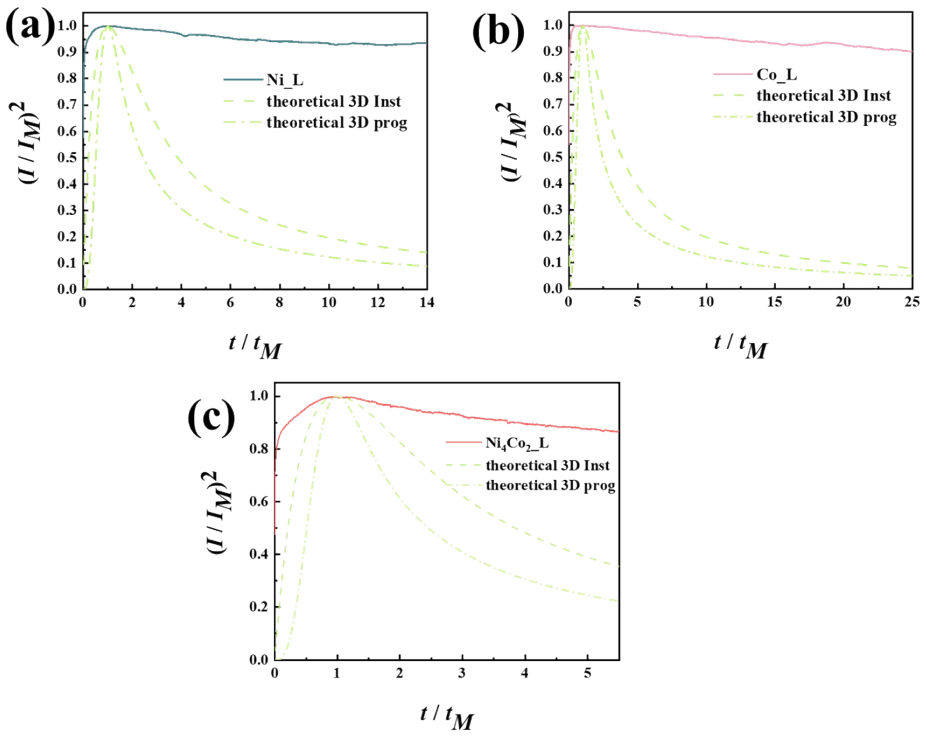

Fig. S1. Non-dimensional $(I / I_M)^2$ vs. (t / t_M) curves of deposition on nickel foam for the electrodeposition of (a) Ni_L, (b) Co_L and Ni_4Co_2_L at -1.4 V_{Ag} .

Equations：

Theoretical 3D Inst : $(I / I_M)^2=1.9542/(t / t_M)*[1-\exp(-1.2564*x)]^2$

Theoretical 3D Prog : $(I / I_M)^2=1.2254/(t / t_M)*[1-\exp(-2.336*x^2)]^2$

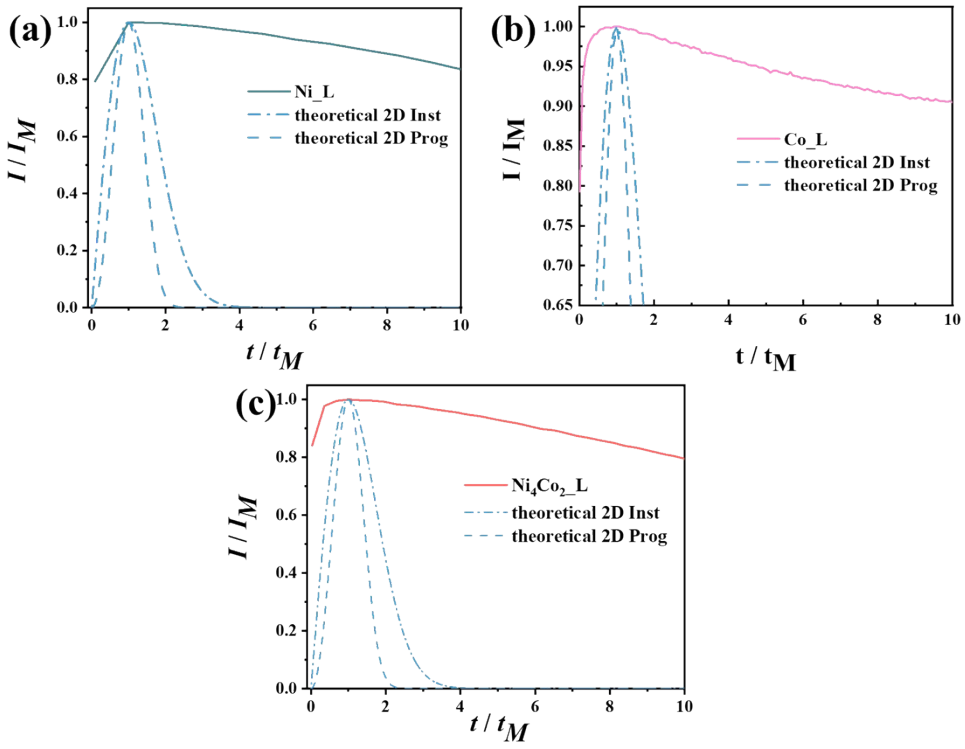

Fig. S2. Non-dimensional $(I / I_M)^2$ vs. (t / t_M) curves for the electrodeposition from (a) Ni_L, (b) Co_L and (c) Ni_4Co_2_L using glassy carbon electrod at -1.4V_{Ag}.

Equations：

Theoretical 2D Inst : (I / IM)= x*{exp((-1/2)*(x^2-1))}

Theoretical 2D Prog : (I / IM)= x^2*{exp((-2/3)*(x^3-1))}

4. XRD

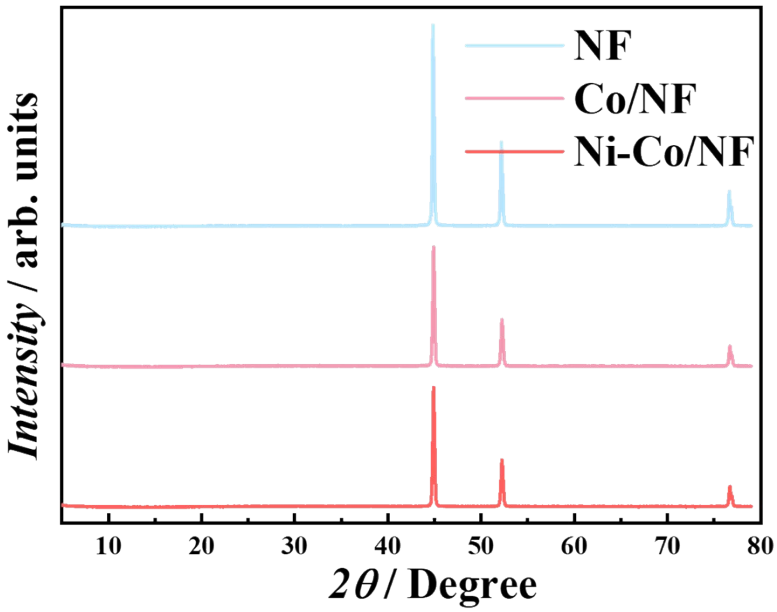

Fig. S3. XRD spectra of Ni-Co on nickel foam.

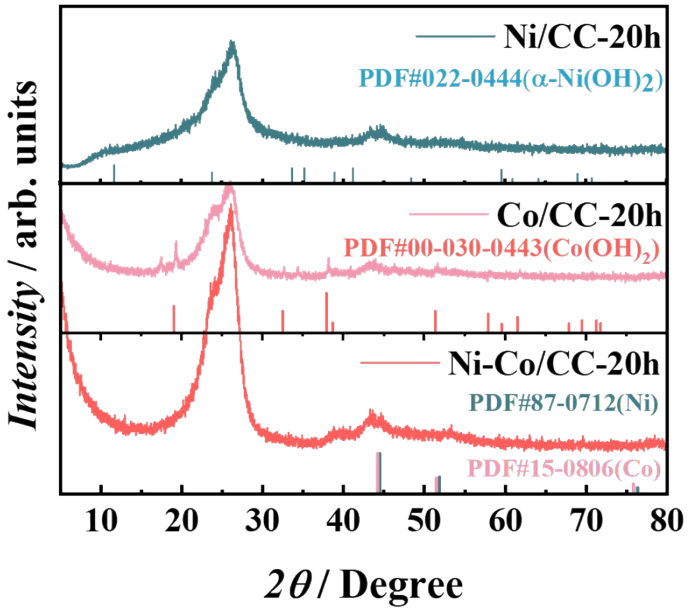

Fig. S4. XRD of Ni/CC, Co/CC, Ni-Co/CC after long-term galvanostatic test.

5. XPS

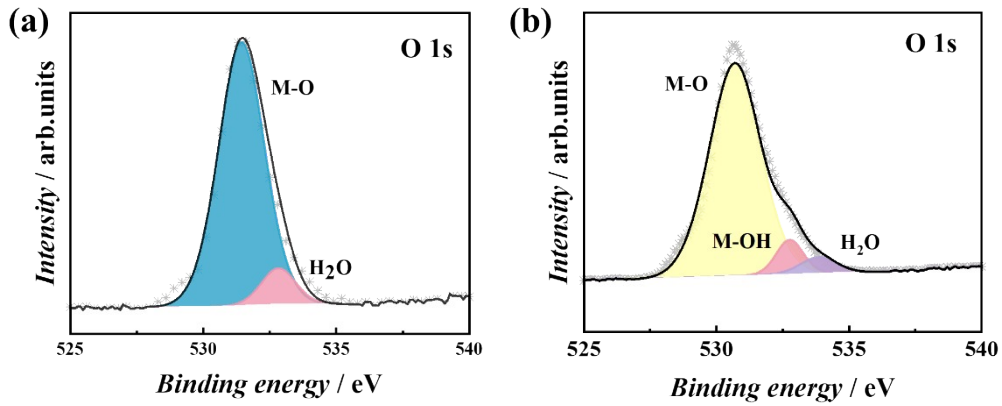

Fig. S5. (a) O 1 s region of Ni-Co in 1M KOH. (b)O 1 s region of Ni-Co after long-term galvanostatic test in 1M KOH.

6. EDX

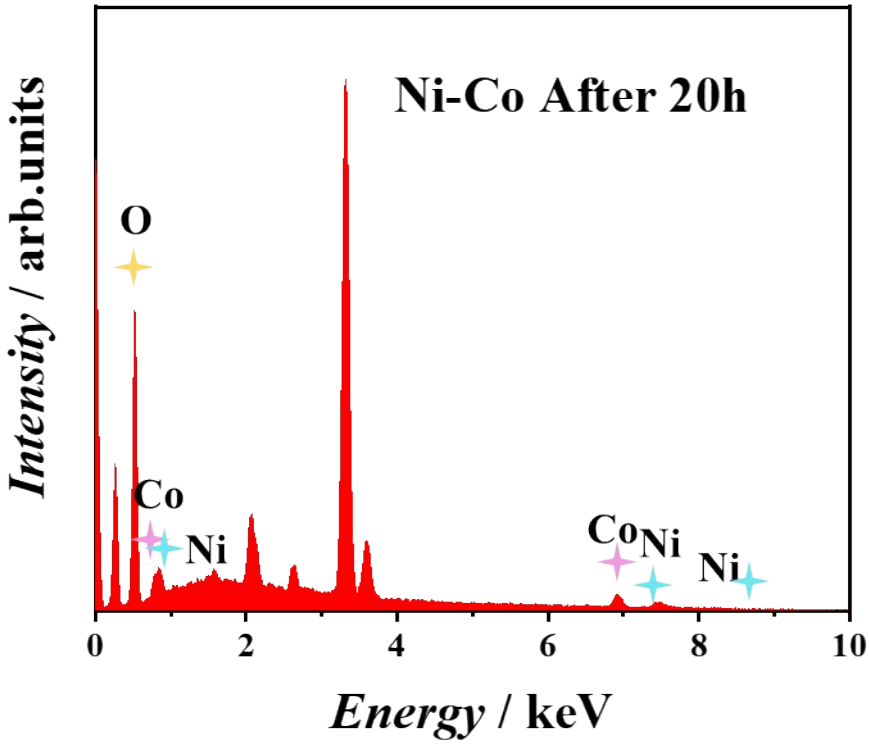

Fig. S6. EDX of Ni Co after long-term galvanostatic HER test.

7. Electrochemistry

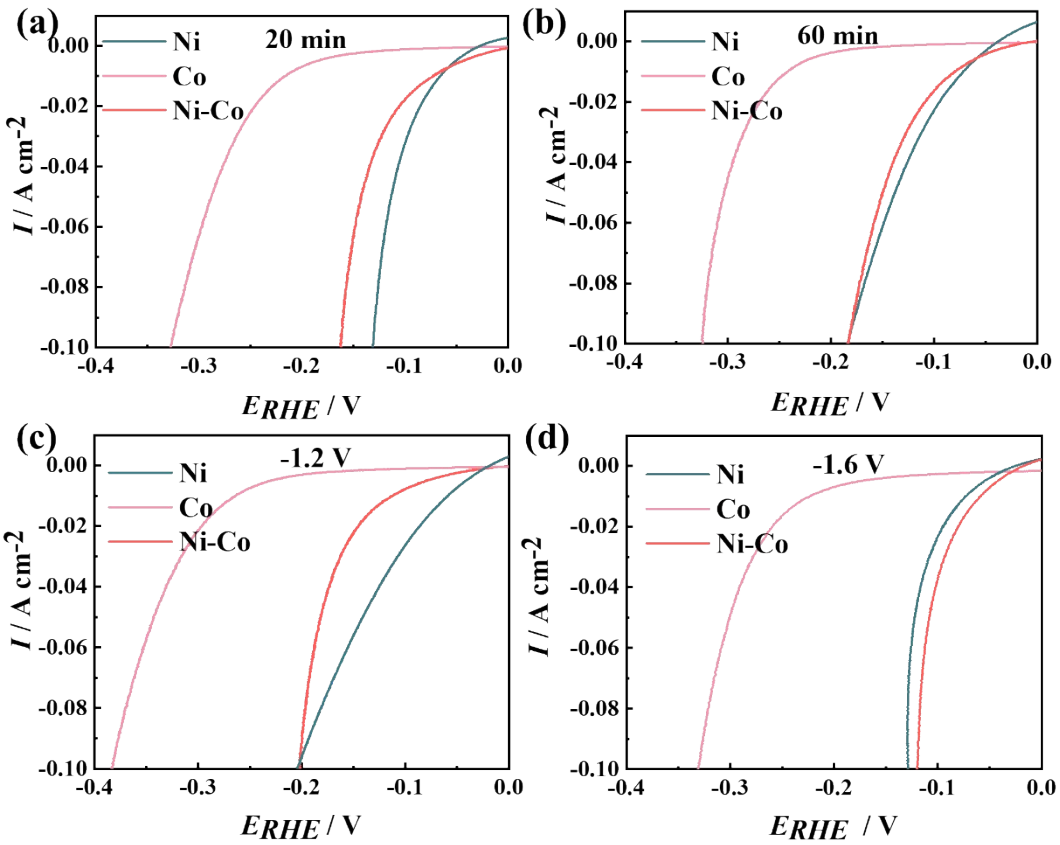

Fig. S7. LSV of Ni, Co and Ni-Co in 1 M KOH 5 mV s^{-1}. The electrodes are electrodeposited under different conditions. (a) 20 min and (b)60 min at -1.4 V_{Ag}; (c) -1.2 V_{Ag} and (d) -1.6 V_{Ag} for 40 min.

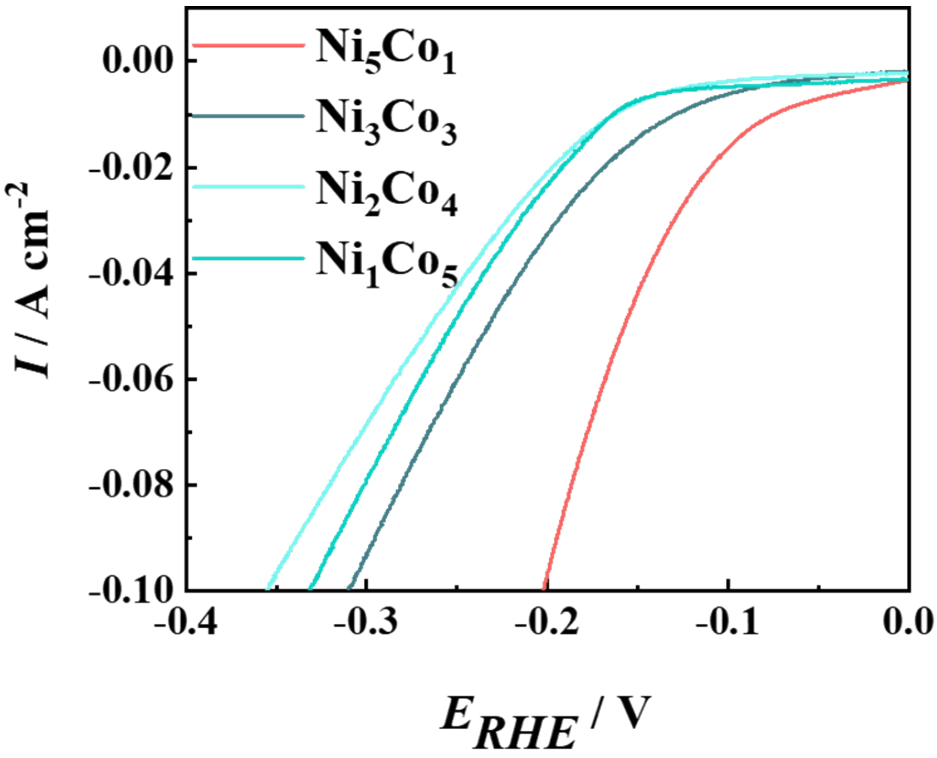

Fig. S8. LSV of Ni-Co in 1 M KOH at 5 mV s^{-1}. The Ni-Co electrodes are electrodeposited using DES containing different proportions of Ni and Co.

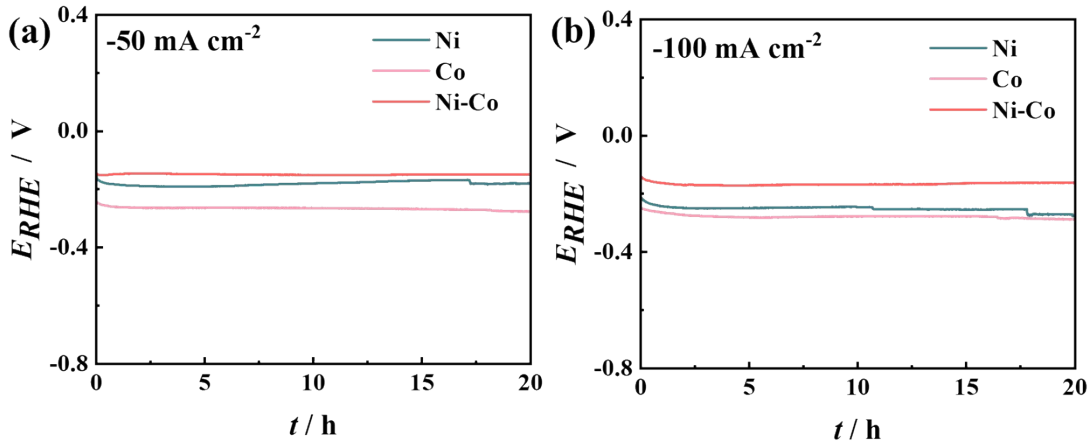

Fig. S9. The galvanostatic HER at (a) -50 mA cm^{-2} and (b) -100 mA cm^{-2} in 1 M KOH.

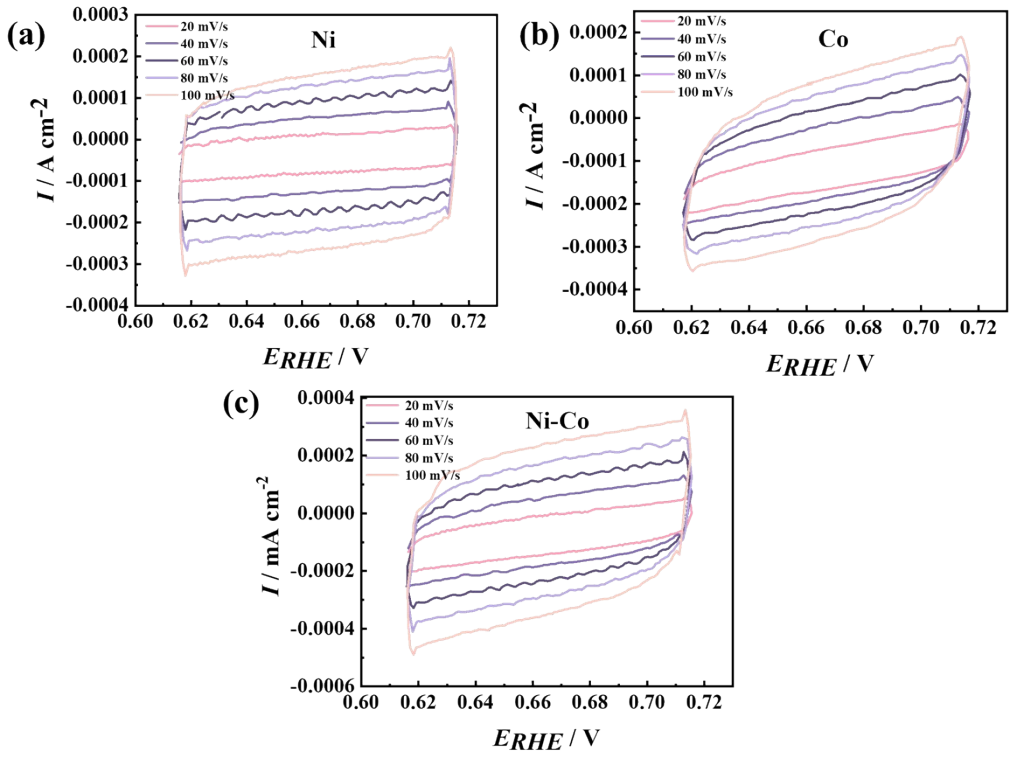

Fig. S10. (a-e) CV of Ni, Co, and Ni-Co at different scan rates (20, 40, 60, 80, and 100 mV s^{-1}) in 0.62 - 0.71 V in 1 M KOH.

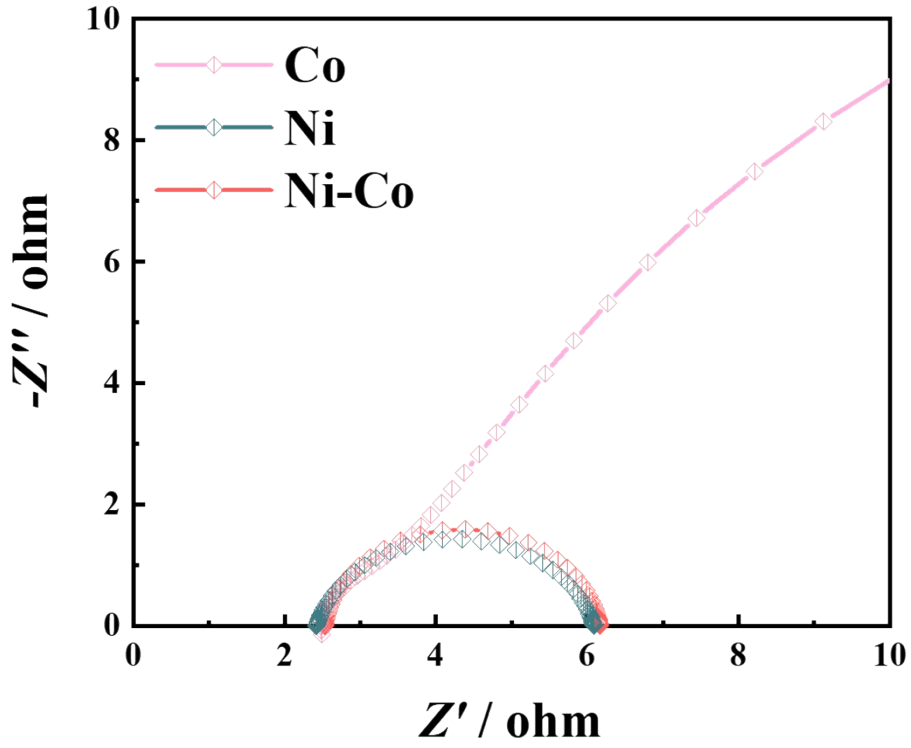

Fig. S11 Nyquist plots (dots) and the fitting curves (line) of the Ni-Co in 1 M KOH at -0.0889 V_{RHE}.

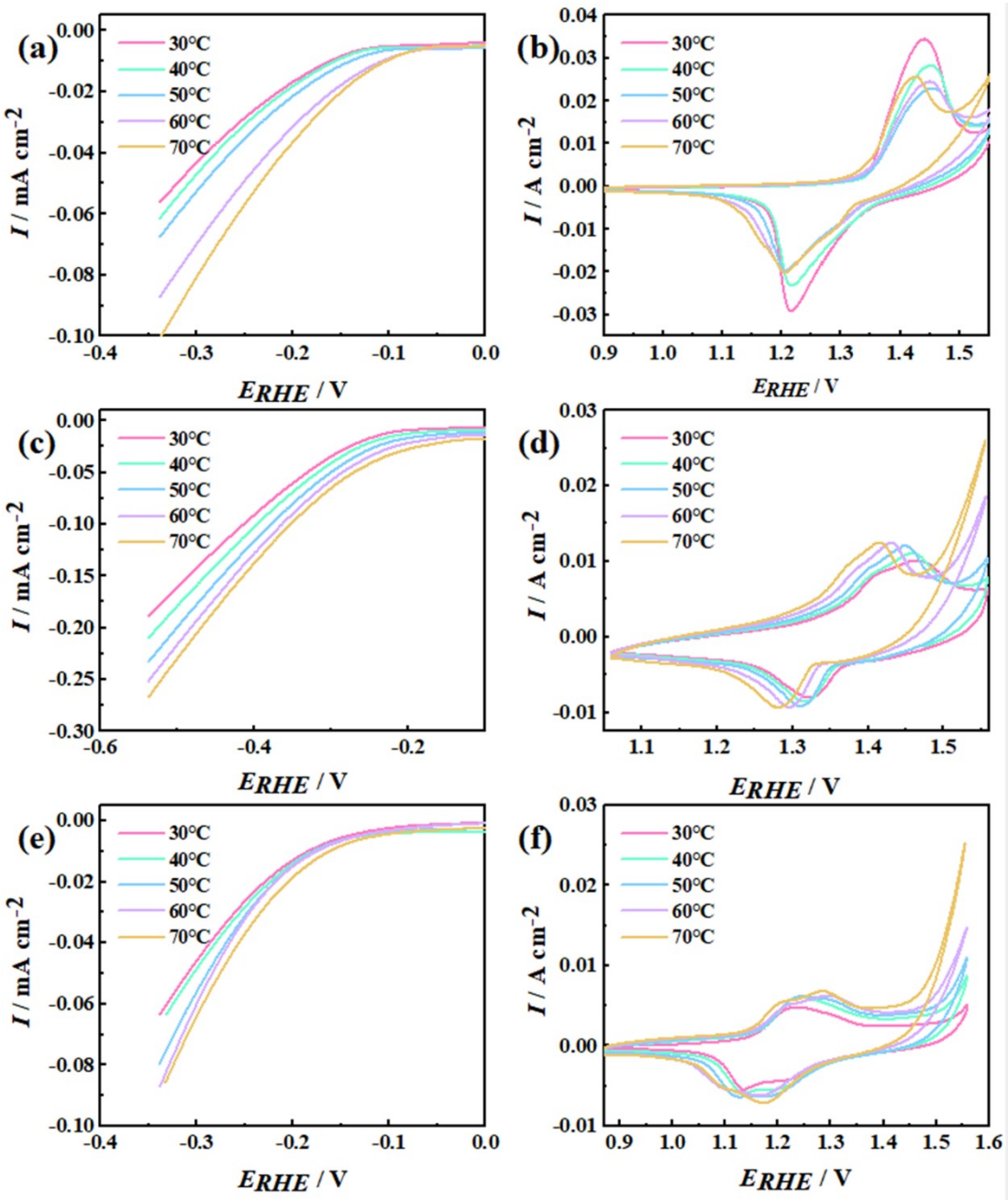

Fig. S12. The LSV and CV of the (a, d) Ni, (b, e) Co, and (c, f) Ni-Co at different temperatures in 1 M KOH at scan rate 5 mV s^{-1}.

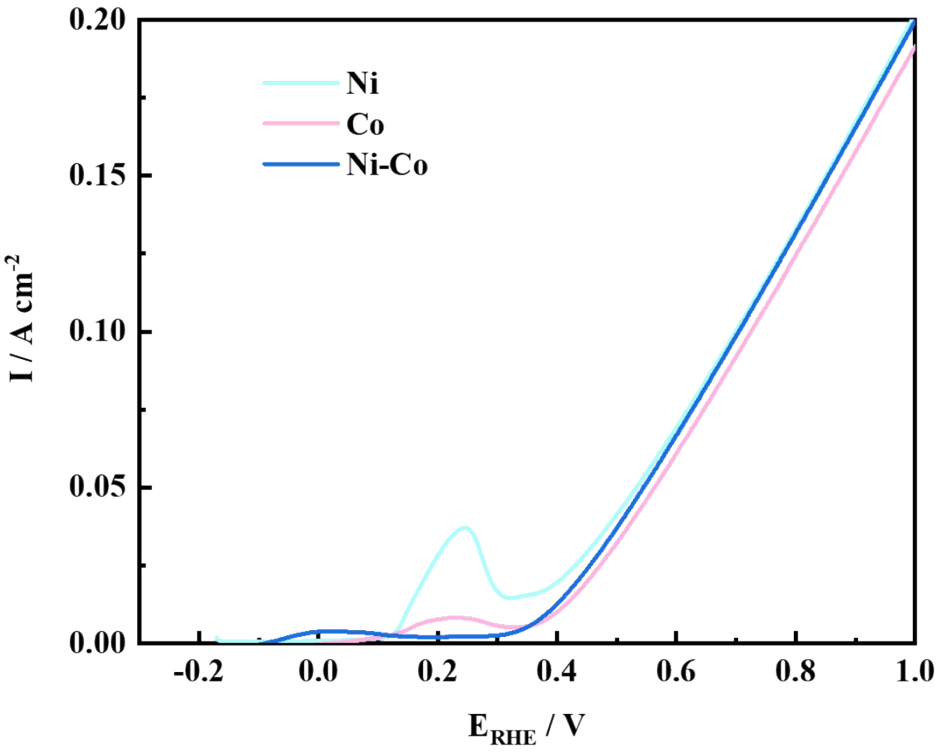

Fig. S13. LSV for OER of the Ni、Co and Ni-Co in 1 M KOH with 5 mV s^{-1}

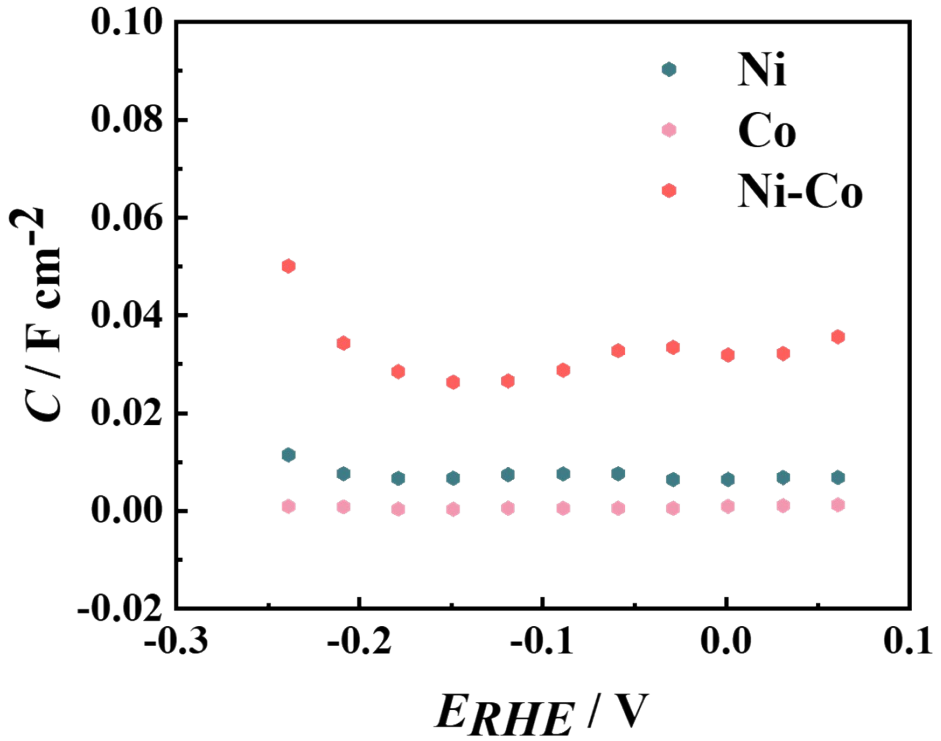

Fig. S14. *C* vs *E* curves of Ni, Co and Ni-Co obtained from electrochemical impedance spectroscopy in 1 M KOH

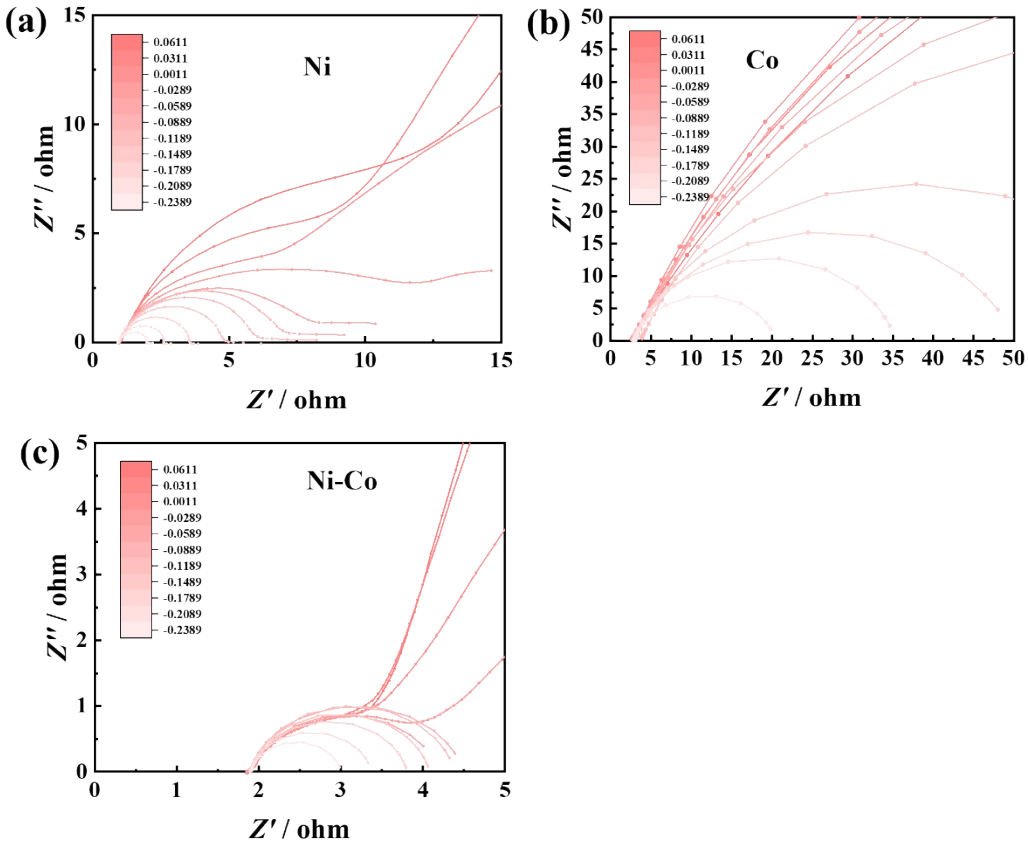

Fig. S15 Nyquist plots of the (a) Ni, (b) Co and (c) Ni-Co at different potentials.

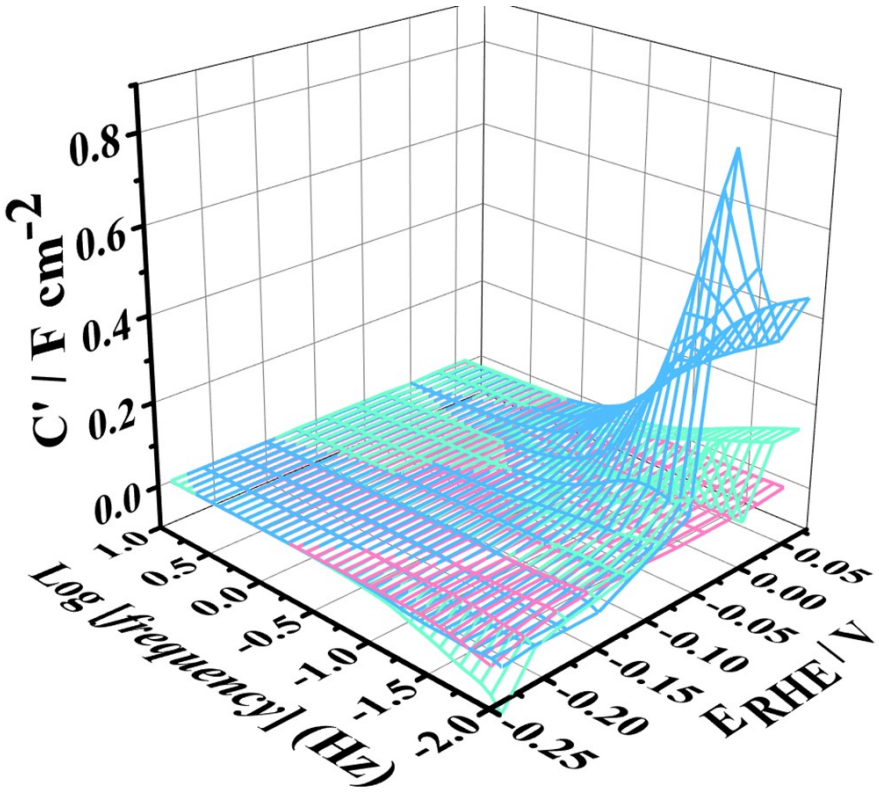

Fig. S16. 3D Bode plots of real area-normalized capacitance (*C*′) vs. frequency vs. potential for Ni, Co and Ni-Co in 1 M KOH.

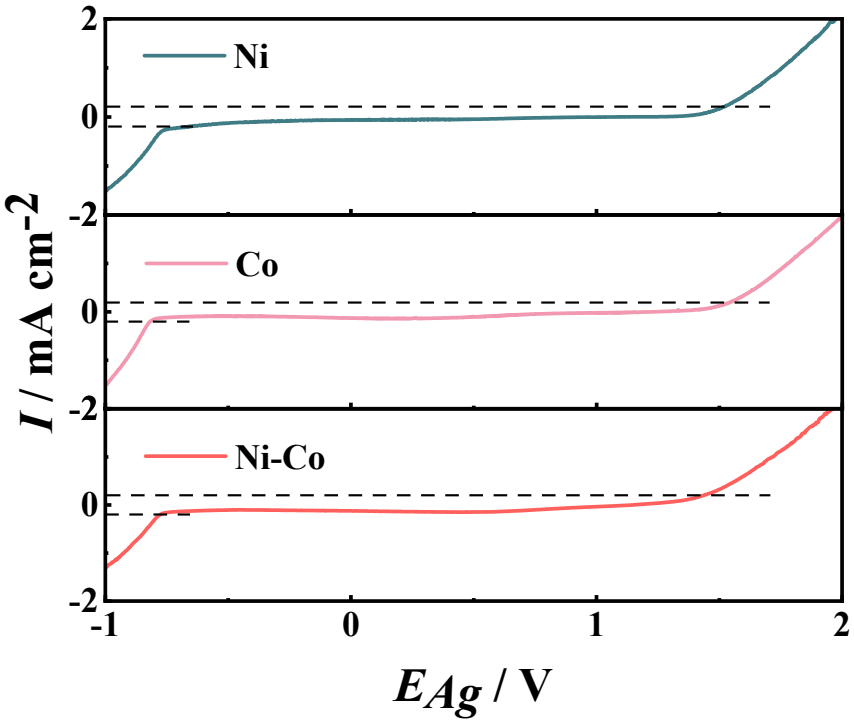

Fig. S17. Cathodic LSV of the DES at 300 K and 50 mV s^{-1}. The working is electrode is a GC.

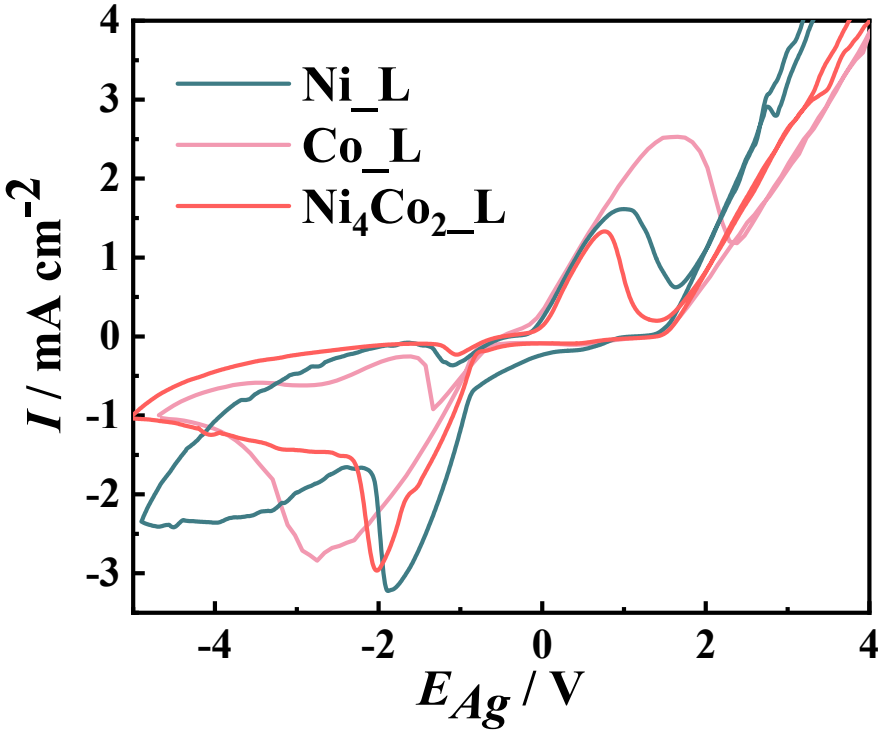

Fig. S18. Cathodic CV of the DES at 300 K and 50 mV s-1. The working is electrode is a GC.

Table S1. EIS fitting results

E / V_{RHE}	R / Ω	Rct / Ω	CPE-T	CPE-P
		Ni		
0.0611	1	22.35	0.023578	0.80265
0.0311	0.98871	15.03	0.021799	0.81021
0.0011	0.97287	10.34	0.019951	0.80664
-0.0289	0.94357	11.19	0.027351	0.73391
-0.0589	0.95412	7.103	0.023818	0.79649
-0.0889	0.95541	6.084	0.018986	0.83994
-0.1189	0.95287	5.078	0.016134	0.86197
-0.1489	0.94839	3.897	0.012915	0.88094
-0.1789	0.94496	2.649	0.010377	0.89715
-0.2089	0.94186	1.696	0.008702	0.90989
-0.2389	0.9375	1.068	0.009077	0.90219
		Co		
0.0611	2.485	326.1	0.008846	0.71671
0.0311	2.723	274.6	0.005383	0.76886
0.0011	2.592	310.5	0.004482	0.78116
-0.0289	2.501	340.9	0.003164	0.75383
-0.0589	2.988	250.7	0.00287	0.77156
-0.0889	2.909	166.2	0.002469	0.79003
-0.1189	3.776	121.2	0.002445	0.80387
-0.1489	2.799	68.13	0.001561	0.78503
-0.1789	2.881	46.9	0.001628	0.79335
-0.2089	2.809	32.29	0.002471	0.85302
-0.2389	2.968	17.36	0.002595	0.85831
		Ni-Co		
0.0611	1.888	2.51	0.081752	0.75838
0.0311	1.884	2.672	0.079144	0.73844
0.0011	1.864	2.625	0.075552	0.73766
-0.0289	1.88	2.481	0.072087	0.77499
-0.0589	1.89	2.323	0.060047	0.81356
-0.0889	1.899	2.565	0.047341	0.84904
-0.1189	1.903	2.474	0.038162	0.86889
-0.1489	1.904	2.174	0.032836	0.87226
-0.1789	1.909	1.884	0.031987	0.86773
-0.2089	1.905	1.455	0.024693	0.88422
-0.2389	1.904	1.092	0.023016	0.88192

8. Activity comparison

Table S2. HER Activity comparison

Catalysts	Method	η at 10 mA cm^{-2} / mV	*Tafel slope* / mV dec^{-1}	Stability/h	References
Ni-Co	Electrodeposition	62	63.5	20	Our work
NiCo nanowires	Template-assisted electrodeposition	103	104	20	1
NiCo	Hydrogen bubble template	54	26	10	2
NiCo	Sputtering	53	68.08	\	3
NiCo/GP	Electrodeposition	107	119	10	4
NiCo-300	Hydrothermal	156	82.7	12	5
SFCA-NiCo	Hydrogel annealing	179	45.6	24	6
CoNi/NF	Electrodeposition	77	94	10	7
NiCo/NiCoOx	Hydrothermal	155	35	10	8
$Co_{0.5}$ $Ni_{0.5}$ P/CC	Hydrothermal + Low-temperature phosphidization	47	34.1	30	9
Ni-Co/Cu	Electrodeposition	131	193	11	10
Ni-Co	Electrodeposition	86.7	69.3	10	11
$Ni_{0.5}Co_{0.5}$	Electroless deposition	36	34.1	96	12

Table S3. Ni $2p_{3/2}$ and Ni $2p_{1/2}$spectral fitting parameters: binding energy (eV), percentage of total area, FWHM value (eV).

	Peak1(eV)	FWHM(eV)	%	Peak2(eV)	FWHM(eV)	%	Peak3(eV)	FWHM(eV)	%
				Ni $2p_{3/2}$					
Ni	853.59	1.260	1.88	856.28	2.822	33.33	862.06	5	32.17
Ni-Co	852.12	1.260	4.07	855.63	2.867	32.19	861.37	5	30.49
Ni-Co-20h	852.94	1.260	2.30	854.95	2.678	34.01	860.86	5	31.20
				Ni $2p_{1/2}$					
Ni	873.58	2.822	16.60	879.33	5	16.03			
Ni-Co	869.41	1.260	2.03	872.93	2.867	16.04	878.67	5	15.19
Ni-Co-20h	872.25	2.678	16.95	878.16	5	15.54			

Table S4. Co $2p_{3/2}$ and Co $2p_{1/2}$spectral fitting parameters: binding energy (eV), percentage of total area, FWHM value (eV).

	Peak1(eV)	FWHM(eV)	%	Peak2(eV)	FWHM(eV)	%	Peak3(eV)	FWHM(eV)	%
				Co $2p_{3/2}$					
Co	779.67	1.633	15.11	781.01	2.786	38.55	786.24	5	18.13
Ni-Co	777.77	0.572	2.03	780.80	3.152	41.21	785.83	5	25.20
Ni-Co-20h	779.06	1.363	10.66	780.34	2.780	41.85	786.20	5	17.80
				Co $2p_{1/2}$					
Co	796.00	2.786	19.18	801.23	5	9.03			
Ni-Co	795.79	3.152	20.01	800.82	5	12.55			
Ni-Co-20h	795.33	2.780	20.85	801.19	5	8.86			

Reference

1. F. Wang, X. Feng, N. Wang, H. Guan, S. Bian, X. Hao and Y. Chen, *Colloids and Surfaces A: Physicochemical and Engineering Aspects*, 2021, **615**.
2. J. Wang, H. Shao, S. Ren, A. Hu and M. Li, *Applied Surface Science*, 2021, **539**.
3. N. S. Gultom, M. Z. Silitonga and D.-H. Kuo, *ACS Applied Energy Materials*, 2022, **5**, 8658-8668.
4. G. B. Darband, M. Aliofkhazraei, A. S. Rouhaghdam and M. A. Kiani, *Applied Surface Science*, 2019, **465**, 846-862.
5. B. Zhang, X. Zhang, Y. Wei, L. Xia, C. Pi, H. Song, Y. Zheng, B. Gao, J. Fu and P. K. Chu, *Journal of Alloys and Compounds*, 2019, **797**, 1216-1223.
6. D. K. Sam, W. Wang, S. Gong, E. K. Sam, X. Lv, J. Wang and J. Liu, *International Journal of Hydrogen Energy*, 2021, **46**, 21525-21533.
7. J. Bai, Q. Sun, Z. Wang and C. Zhao, *Journal of The Electrochemical Society*, 2017, **164**, H587.
8. X. Yan, K. Li, L. Lyu, F. Song, J. He, D. Niu, L. Liu, X. Hu and X. Chen, *ACS Applied Materials & Interfaces*, 2016, **8**, 3208-3214.
9. X. Zhang, W. Gu and E. Wang, *Journal of Materials Chemistry A*, 2017, **5**, 982-987.
10. A. Maurya, S. Suman, A. Bhardwaj, L. Mohapatra and A. K. Kushwaha, *Electrocatalysis*, 2022, **14**, 68-77.
11. X. Zhang, Y. Li, Y. Guo, A. Hu, M. Li, T. Hang and H. Ling, *International Journal of Hydrogen Energy*, 2019, **44**, 29946-29955.
12. P. Zou, J. Li, Y. Zhang, C. Liang, C. Yang and H. J. Fan, *Nano Energy*, 2018, **51**, 349-357.